Japanese Journal of Applied Physics **REGULAR PAPER**

Correlated Time-Series Reconstruction in Carbon Composites Using a Kalman Filtering Framework

Anshuman Mondal[1], Anowarul Habib[2]*

[1]*Department of Electronics and Electrical Engineering, Indian Institute of Technology Guwahati, India*
[2]*Department of Physics and Technology, UiT The Arctic University of Norway, 9037 Tromsø, Norway*

Accurate reconstruction of acoustic emission (AE) signals is essential for reliable structural health monitoring, yet sensor outages and missing data remain common in practical deployments. We propose a recursive covariance-based Kalman filtering framework that models inter-sensor correlations to reconstruct nearly complete AE waveforms from highly sparse observations. The method uses only a 5% seed segment of the target signal and auxiliary measurements from neighboring sensors. It performs sequential prediction and correction while preserving full state covariance. This ensures stable estimation even under anisotropy and noise. Experiments on impact-generated AE in carbon-fiber-reinforced polymer plates demonstrate high reconstruction fidelity, achieving SSIM greater than 0.9, and correlation of 0.85–0.93 across 82 datasets.

1. Introduction

Anisotropic composite materials, most notably carbon-fiber-reinforced polymers (CFRPs), are widely adopted in aerospace, automotive, and wind-energy structures because of their high stiffness and strength-to-weight ratio.[1–3)] Despite these advantages, CFRPs are susceptible to localized damage, including delamination, interfacial debonding, matrix cracking, and fiber rupture. These defects often initiate under low-velocity impacts or accumulate under cyclic loading, and, if undetected, can degrade structural performance and precipitate catastrophic failure. Structural health monitoring (SHM) mitigates this risk by enabling in-situ detection and localization of damage. Among SHM modalities, acoustic emission (AE) is particularly effective for capturing the transient elastic waves generated at the onset and growth of damage, providing information about initiation mechanisms and propagation paths. SHM systems commonly use sparse arrays of ultrasonic transducers that can operate in active mode, where actuators inject guided ultrasonic waves (GUWs) for interrogation, or in passive mode, where the array listens for AE generated by impacts or evolving flaws.[4,5)] Permanently installed arrays allow continuous or condition-based monitoring throughout a structure's service life.

*E-mail: anowarul.habib@uit.no

Localizing AE sources in composites is challenging. In isotropic plates, three-sensor triangulation works because wave speed is direction-independent. In anisotropic laminates, wave speed varies with direction and frequency, set by stacking sequence and material symmetry—so standard triangulation fails, and anisotropy must be modeled. Many methods exist,[6,7] but two issues persist: (i) computational cost grows rapidly with sensor count/model complexity, and (ii) accuracy is highly sensitive to time-of-flight (TOF) errors. Small TOF uncertainties from ambient variation, mode conversion, dispersion, system bias, or noise can yield large localization errors.

Missing data are common in large-scale sensor networks, arising from pre-trigger truncation, DAQ buffer overruns, brief loss of coupling, ADC saturation/blanking, synchronization glitches, EMI, or sensor wear/damage in harsh environments (heat, humidity, moisture ingress, mechanical fatigue). These gaps degrade downstream processing and can lead to incorrect decisions. Prior work on data recovery in SHM spans four main families—interpolation, compressive sensing (CS), statistical/ML, and time-series models.[8–10] Interpolation (least-squares, simple imputation, adjacent-sensor correlation) can fill short gaps but assumes linearity and ignores measurement uncertainty, yielding large errors for long or noisy gaps.[11–13] CS methods perform well for sparse (or near-sparse) vibration spectra, but many SHM/AE signals are not uniformly sparse across conditions.[14,15] Statistical/ML approaches (PCA, distribution regression, neural networks) capture complex relations yet typically require large training sets and careful domain transfer.[16–18] Time-series models ensure sequential consistency but can become computationally heavy when scaled to multi-sensor, anisotropic, noisy settings.

Motivated by these limitations, we reconstruct nearly complete gaps ($\approx 95\%$) in a target waveform using a standard Kalman filter (KF) that fuses information from auxiliary channels. A short seed segment ($\approx 5\%$) of the target trace initializes the state and covariance; the KF then predicts–updates sequentially in time using contemporaneous auxiliary observations, thereby avoiding heavy multi-sensor optimization while retaining full probabilistic consistency. We specifically chose the full KF over a lightweight variant because "lightweight" simplifications (e.g., reduced state, diagonalized/fixed covariances, fixed (Q/R) can amplify model-mismatch, underestimate uncertainty, and drift during long measurement gaps, especially with anisotropy, dispersion, and nonstationary noise. In contrast, the standard KF preserves the complete covariance structure and supports adaptive/tuned Q, R, yielding more stable reconstructions that better preserve amplitude, morphology, and temporal features of impact-generated AE. We quantify fidelity with MSE, SSIM, and Pearson correlation, demonstrating preservation of amplitude, morphology, and key temporal features of impact-generated

AE. The method explicitly models uncertainty, leverages cross-channel structure, and remains efficient for sparse, real-time SHM deployments with constrained bandwidth, power, or channel count. Figure 1 presents the flow diagram of the study: AE signals from S_1 and S_2 are time-aligned with a partial (5%) segment of the target trace S_n (n can be any sensor). This segment initializes a linear state-space / Kalman filter (state and covariance). The recursive loop then predicts the remaining samples of S_n in a time-progressive manner, using S_1 and S_2 as auxiliaries; corrections are applied when measurements are available, otherwise prediction advances the estimate. Reconstruction fidelity is quantified with MSE, SSIM, and Pearson correlation, confirming preservation of amplitude and waveform morphology.

2. Data Acquisition and Preprocessing

Experimental validation was carried out on a 60 cm × 60 cm CFRP panel with a nominal thickness of 20 mm, chosen to represent a thin, anisotropic plate typical of lightweight structural applications (Figure 2).[3,19] To emulate a reproducible low-energy impact event, a Teflon sphere of diameter 13.4 mm (mass $\approx 10g$) was released from a height of $\approx$ 30 cm onto a randomly selected point on the panel surface. A sparse array of five acoustic sensors was bonded to the panel. The sensor positions were chosen to (i) provide geometric diversity for robust multilateration, (ii) limit wiring and added mass on the panel, and (iii) maintain good coverage of the test area. Following each impact, the transient AE responses were recorded synchronously across all channels for subsequent source localization. For a representative trial, the effects at (x, y) = (30 cm, 35 cm) were assessed by analyzing the time-domain waveforms measured at the five sensors. Arrival times were picked using a consistent thresholding/cross-correlation strategy, and the source location was estimated from the differential time-of-arrival data using standard multilateration on a 2-D plate. The corresponding sensor coordinates used in the reconstruction are provided in the accompanying materials.

3. Mathematical Background of the Proposed Algorithm

The proposed method reconstructs an incomplete AE waveform (S_3) using a discrete-time linear state–space model with a two-dimensional state and a Kalman filter. Only the first 5% of S_3 is observed; the remaining 95% is reconstructed using auxiliary signals from Sensors S_1 and S_2.

3.1 State–Space Model

The hidden state consists of the true $S3$ amplitude and its latent "velocity" term:

$$\mathbf{x}_k = \begin{bmatrix} x_k^{(1)} \\ x_k^{(2)} \end{bmatrix} \in \mathbb{R}^2, \tag{1}$$

where $x_k^{(1)}$ represents the instantaneous amplitude of S_3 and $x_k^{(2)}$ models its local temporal rate of change.

The system dynamics follow a constant-velocity model:

$$\mathbf{x}_k = \underbrace{\begin{bmatrix} 1 & 1 \\ 0 & 1 \end{bmatrix}}_{\mathbf{A}} \mathbf{x}_{k-1} + \underbrace{\begin{bmatrix} b_1 & b_2 & b_3 & b_4 \\ c_1 & c_2 & c_3 & c_4 \end{bmatrix}}_{\mathbf{B}} \mathbf{u}_k + \mathbf{w}_k, \tag{2}$$

$$\mathbf{z}_k = \underbrace{\begin{bmatrix} 1 & 0 \end{bmatrix}}_{\mathbf{H}} \mathbf{x}_k + \mathbf{v}_k, \tag{3}$$

where $\mathbf{A} \in \mathbb{R}^{2\times2}$, $\mathbf{B} \in \mathbb{R}^{2\times4}$, $\mathbf{H} \in \mathbb{R}^{1\times2}$, and $\mathbf{w}_k \sim \mathcal{N}(0, \mathbf{Q})$, $\mathbf{v}_k \sim \mathcal{N}(0, \mathbf{R})$ are Gaussian process and measurement noises, respectively. The form of $\mathbf{A}$ matches the exact constant-velocity transition used in the implementation.

3.2 Input Vector Construction

Auxiliary information from S_1 and S_2 is encoded as:

$$\mathbf{u}_k = \begin{bmatrix} S1_k \\ S2_k \\ \Delta S1_k \\ \Delta S2_k \end{bmatrix}, \qquad \Delta S1_k = S1_k - S1_{k-1}, \quad \Delta S2_k = S2_k - S2_{k-1}. \tag{4}$$

The control matrix $\mathbf{B} \in \mathbb{R}^{2\times4}$ models how the sensor amplitudes and their temporal gradients influence the S3 amplitude and its latent velocity.

3.3 Kalman Filter Recursion

Prediction:

$$\hat{\mathbf{x}}_{k|k-1} = \mathbf{A}\,\hat{\mathbf{x}}_{k-1|k-1} + \mathbf{B}\,\mathbf{u}_k, \tag{5}$$

$$\mathbf{P}_{k|k-1} = \mathbf{A}\,\mathbf{P}_{k-1|k-1}\mathbf{A}^T + \mathbf{Q}. \tag{6}$$

Update (performed only within the first 5% where $S3$ is observed):

$$\mathbf{K}_k = \mathbf{P}_{k|k-1}\mathbf{H}^T \left(\mathbf{H}\mathbf{P}_{k|k-1}\mathbf{H}^T + \mathbf{R}\right)^{-1}, \tag{7}$$

$$\hat{\mathbf{x}}_{k|k} = \hat{\mathbf{x}}_{k|k-1} + \mathbf{K}_k \left(\mathbf{z}_k - \mathbf{H}\hat{\mathbf{x}}_{k|k-1}\right), \tag{8}$$

$$\mathbf{P}_{k|k} = (\mathbf{I} - \mathbf{K}_k\mathbf{H})\mathbf{P}_{k|k-1}. \tag{9}$$

3.4 Filter Initialization

The first 5% of $S3$ is used for initialization:

$$\hat{\mathbf{x}}_{0|0} = \begin{bmatrix} S3(0) \\ 0 \end{bmatrix}, \qquad \mathbf{P}_{0|0} = \sigma_{S3}^2\mathbf{I},$$

where the second component is initialized to zero velocity, consistent with the implementation.

3.5 Reconstruction of Missing Samples

After the initial 5% segment, no further measurements of S_3 are available. Thus, the filter performs *prediction only* for the remaining 95%:

$$\hat{\mathbf{x}}_{k|k-1} = \mathbf{A}\hat{\mathbf{x}}_{k-1|k-1} + \mathbf{B}\mathbf{u}_k, \qquad \hat{S3}(k) = \mathbf{H}\hat{\mathbf{x}}_{k|k-1}.$$

This recursive prediction produces a complete reconstruction of the missing portion of the S3 waveform, guided by the auxiliary sensor data and their temporal gradients.

4. Results and Discussion

The signals have been reconstructed using the devised strategy and overlapped and placed with the ground reality of S_3 for two of the samples out of 82 sensors' data (namely 1^{st} and 5^{th} samples have been illustrated in Figure 3. For two representative impact events, the reconstructed S_3 signals obtained from the Kalman filter closely matched the corresponding measured waveforms (Fig. 3a and b). In both cases, the predicted traces successfully reproduced the waveform morphology and peak arrival times, indicating strong agreement with the true signal. This consistency demonstrates that the Kalman filter can reliably recover missing AE information when supported by correlated inputs from auxiliary sensors. The reconstructed signals were compared with the ground truth using Mean Squared Error (MSE), Structural Similarity Index (SSIM), and Pearson correlation coefficient. Figure 4 shows the MSE variation across all 82 samples. In the majority of cases, the MSE remained below 0.01, indicating a small deviation between the reconstructed and the actual S_3 waveforms. A cluster of samples exhibited MSE in the range of 0.001–0.006, with occasional higher values (up to ≈ 0.018) for samples containing sharp impact transients or higher-frequency content. The low error magnitude confirms that the filter effectively utilizes S_1 and S_2 trends to estimate the missing S_3 dynamics. The SSIM values, plotted in Fig. 5, consistently remained above 0.85, with several samples exceeding 0.92. This demonstrates that the temporal structure and shape of the AE waveform are preserved during reconstruction. SSIM captures local variations in peaks and rise times, and the high scores indicate that the predicted waveform follows the ref-

erence morphology closely. Samples with slightly lower SSIM values (0.85–0.88) correspond to instances where the original S_3 signal contained abrupt discontinuities, which are inherently harder to model using a linear state-space formulation. The Pearson correlation coefficients, shown in Fig. 6, further illustrate the strong agreement between reconstructed and ground-truth waveforms. Most samples achieved correlation values above 0.80, with many exceeding 0.90. High correlation implies excellent alignment of peak locations and overall waveform trends. A few samples exhibited moderate correlation (0.72–0.78), particularly where signal energy was concentrated in narrow, high-amplitude spikes. Even in such cases, the filter maintained the correct overall trend, demonstrating good robustness.

Overall, the combination of low MSE, high SSIM, and high correlation confirms that the proposed Kalman-based approach successfully reconstructs incomplete AE signals by leveraging information from auxiliary sensors. Importantly, the method shows consistent performance across a large dataset, despite the variability in impact conditions and waveform characteristics. The filter not only captures the amplitude evolution but also preserves the waveform shape, making it highly suitable for downstream tasks such as impact detection, classification, and localization. The lightweight computational footprint further enables real-time deployment in embedded SHM systems.

5. Conclusion

The proposed Kalman filter–based framework provides an effective solution for reconstructing incomplete AE signals in CFRP composites. By using only 5% of the target waveform and incorporating correlated information from auxiliary sensors through a compact state-space model, the method successfully restores amplitude, waveform shape, and key temporal features while suppressing noise. Performance metrics—including low MSE values, SSIM scores above 0.88, and correlation coefficients exceeding 0.86—demonstrate that the reconstructed signals closely match the true measurements across various impact events. The approach is computationally efficient, sensor-efficient, and well-suited for real-time SHM scenarios where partial signal loss or limited sensing is common. Overall, this reconstruction strategy offers a practical and robust pathway for recovering corrupted AE data and strengthens the reliability of AE-based monitoring in composite structures.

Data Availability

The datasets generated and analyzed during the current study are available from the corresponding author on reasonable request.

Conflict of Interest

The authors declare no conflicts of interest.

References

1) Wieslaw Staszewski, Christian Boller, and Geoffrey R Tomlinson. *Health monitoring of aerospace structures: smart sensor technologies and signal processing*. John Wiley & Sons, 2004.
2) Charles R Farrar and Nick AJ Lieven. Damage prognosis: the future of structural health monitoring. *Philosophical Transactions of the Royal Society A: Mathematical, Physical and Engineering Sciences*, 365(1851):623–632, 2007.
3) Nur MM Kalimullah, Shivam Ojha, Maciej Radzieński, Amit Shelke, and Anowarul Habib. A probabilistic machine learning framework for stiffness tensor estimation of carbon composite laminate. *Mechanical Systems and Signal Processing*, 223:111872, 2025.
4) Ajit K Mal, Frank Shih, and Sauvik Banerjee. Acoustic emission waveforms in composite laminates under low velocity impact. In *Smart Nondestructive Evaluation and Health Monitoring of Structural and Biological Systems II*, volume 5047, pages 1–12. SPIE, 2003.
5) E Dehghan Niri, A Farhidzadeh, and S Salamone. Nonlinear kalman filtering for acoustic emission source localization in anisotropic panels. *Ultrasonics*, 54(2):486–501, 2014.
6) Francesco Ciampa and Michele Meo. A new algorithm for acoustic emission localization and flexural group velocity determination in anisotropic structures. *Composites Part A: Applied Science and Manufacturing*, 41(12):1777–1786, 2010.
7) Tribikram Kundu, Samik Das, and Kumar V Jata. Detection of the point of impact on a stiffened plate by the acoustic emissiontechnique. *Smart Materials and Structures*, 18(3):035006, 2009.
8) YF Luo, ZW Ye, XN Guo, XH Qiang, and XM Chen. Data missing mechanism and missing data real-time processing methods in the construction monitoring of steel structures. *Advances in Structural Engineering*, 18(4):585–601, 2015.
9) Yuequan Bao, Yan Yu, Hui Li, Xingquan Mao, Wenfeng Jiao, Zilong Zou, and Jinping Ou. Compressive sensing-based lost data recovery of fast-moving wireless sensing for structural health monitoring. *Structural Control and Health Monitoring*, 22(3):433–448, 2015.
10) Zilong Zou, Yuequan Bao, Hui Li, Billie F Spencer, and Jinping Ou. Embedding compressive sensing-based data loss recovery algorithm into wireless smart sensors for

structural health monitoring. *IEEE Sensors Journal*, 15(2):797–808, 2014.

11) Steven J Hadeed, Mary Kay O'rourke, Jefferey L Burgess, Robin B Harris, and Robert A Canales. Imputation methods for addressing missing data in short-term monitoring of air pollutants. *Science of the Total Environment*, 730:139140, 2020.
12) Julie Josse, Marie Chavent, Benot Liquet, and François Husson. Handling missing values with regularized iterative multiple correspondence analysis. *Journal of classification*, 29(1):91–116, 2012.
13) Zeyu Zhang and Yaozhi Luo. Restoring method for missing data of spatial structural stress monitoring based on correlation. *Mechanical Systems and Signal Processing*, 91:266–277, 2017.
14) Yong Huang, James L Beck, Stephen Wu, and Hui Li. Bayesian compressive sensing for approximately sparse signals and application to structural health monitoring signals for data loss recovery. *Probabilistic Engineering Mechanics*, 46:62–79, 2016.
15) Yongchao Yang and Satish Nagarajaiah. Harnessing data structure for recovery of randomly missing structural vibration responses time history: Sparse representation versus low-rank structure. *Mechanical Systems and Signal Processing*, 74:165–182, 2016.
16) François Husson and Julie Josse. Handling missing values in multiple factor analysis. *Food quality and preference*, 30(2):77–85, 2013.
17) Zhicheng Chen, Yuequan Bao, Hui Li, and Billie F Spencer Jr. A novel distribution regression approach for data loss compensation in structural health monitoring. *Structural Health Monitoring*, 17(6):1473–1490, 2018.
18) Seongwoon Jeong, Max Ferguson, Rui Hou, Jerome P Lynch, Hoon Sohn, and Kincho H Law. Sensor data reconstruction using bidirectional recurrent neural network with application to bridge monitoring. *Advanced engineering informatics*, 42:100991, 2019.
19) Anshuman Mondal, Shivam Ojha, Amit Shelke, and Anowarul Habib. Reconstruction of corrupted signal in carbon composite using kalman filter. *The Symposium on Ultrasonic Electronics*, 49(2P2-10), 2025.

Fig. 1: Workflow for AE waveform reconstruction with a Kalman filter. S_1 and S_2 are aligned with a seed segment of target sensor S_n, initializing the state and covariance. Prediction and correction proceed recursively, producing the reconstructed waveform.

Fig. 2: Experimental setup for impact testing on a carbon-fiber composite plate. The 60 cm × 60 cm composite specimen is instrumented with five surface-mounted sensors S_1 to S_5 positioned near the plate edges. A Teflon sphere is released from a height of 30 cm above the specimen to generate controlled impact events. This configuration enables assessment of sensor responses and signal propagation characteristics under repeatable impact loading conditions.

Fig. 3: Comparison of the actual and Kalman-reconstructed S_3 waveforms for two impact events, shown in (a) and (b). In both cases, the predicted signals (dashed orange) closely follow the measured waveforms (solid blue), accurately reproducing the waveform morphology and peak arrival times. These results demonstrate the Kalman filter's ability to recover missing AE data by leveraging information from auxiliary sensors.

Fig. 4: MSE comparison between original and reconstructed signal shows lower values, indicating a proper fit.

Fig. 5: Structural Similarity Index (SSIM) comparison between the measured and reconstructed S3 signals. High SSIM confirms the preservation of waveform structure.

Fig. 6: Pearson correlation analysis between actual and reconstructed S3 values. The strong correlation demonstrates the effectiveness of the predictive model.

Jpn. J. Appl. Phys. **REGULAR PAPER**

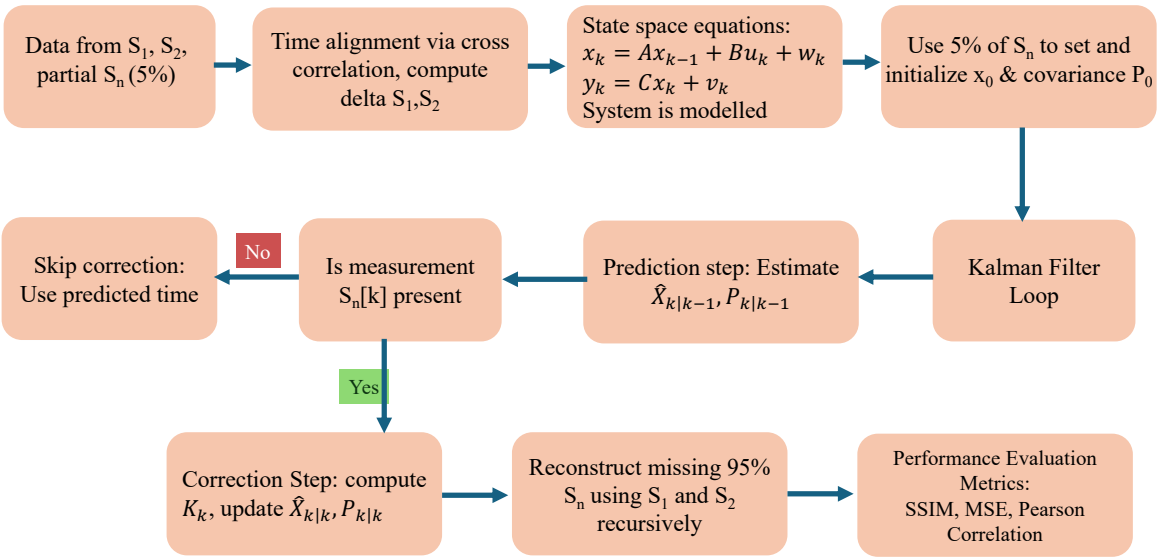

Fig. 1.

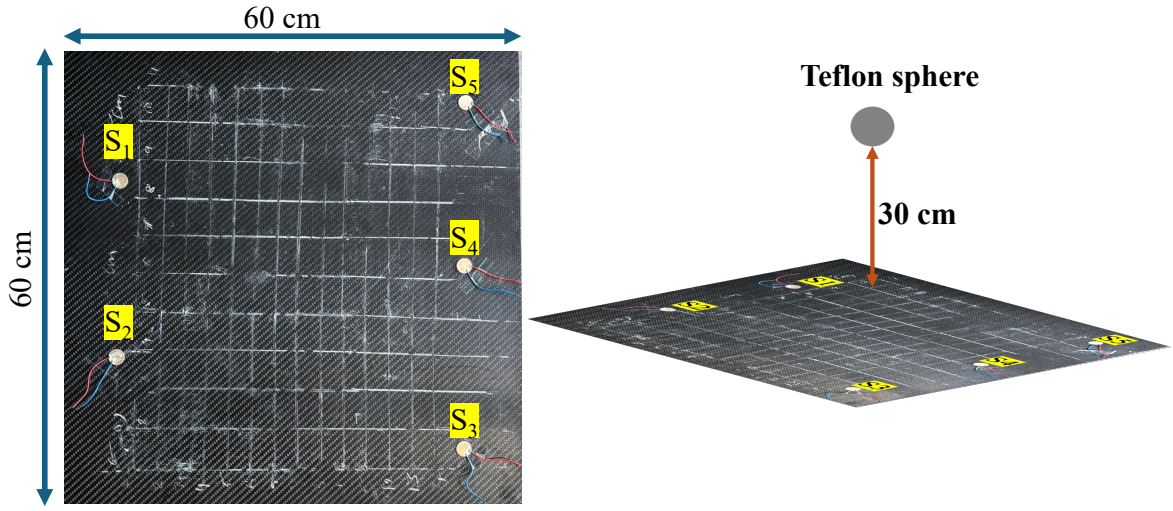

Fig. 2.

Jpn. J. Appl. Phys. **REGULAR PAPER**

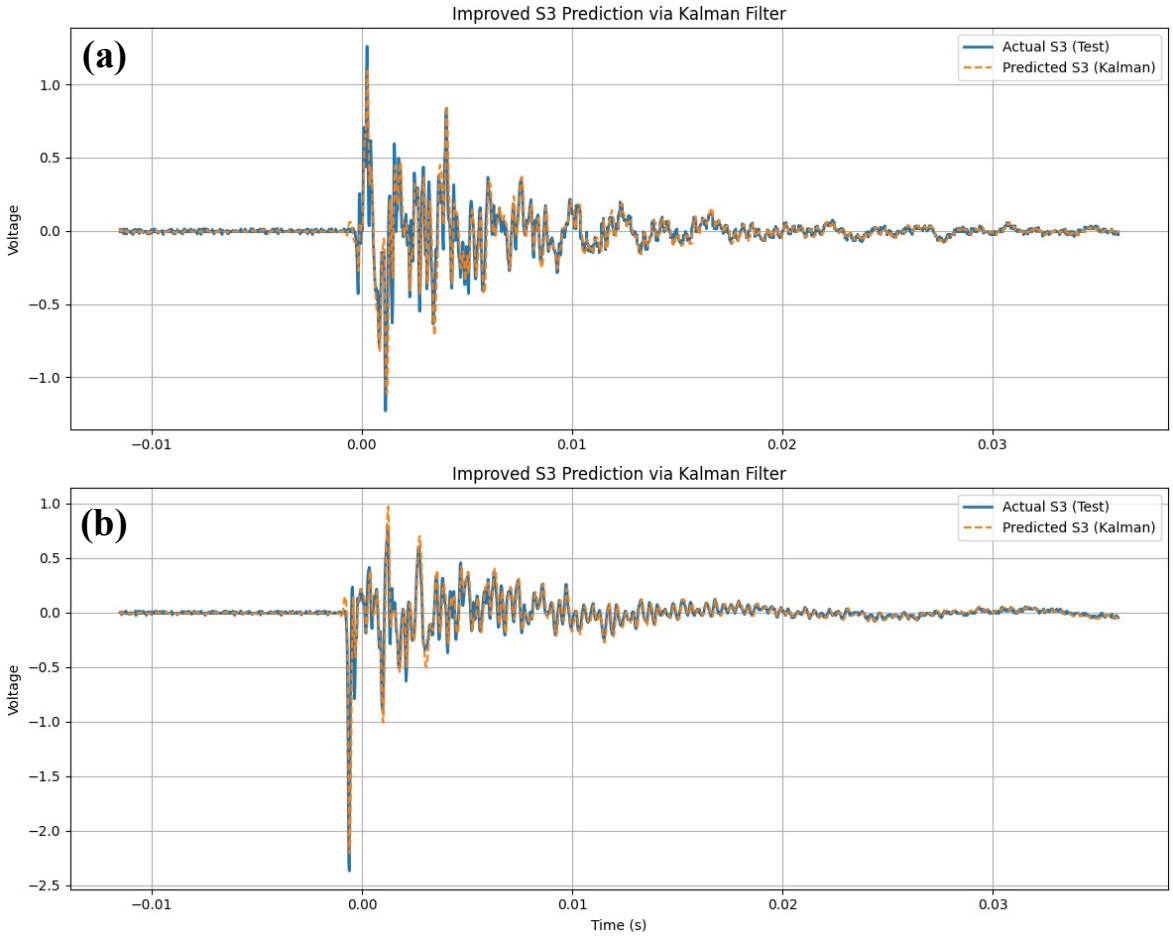

Fig. 3.

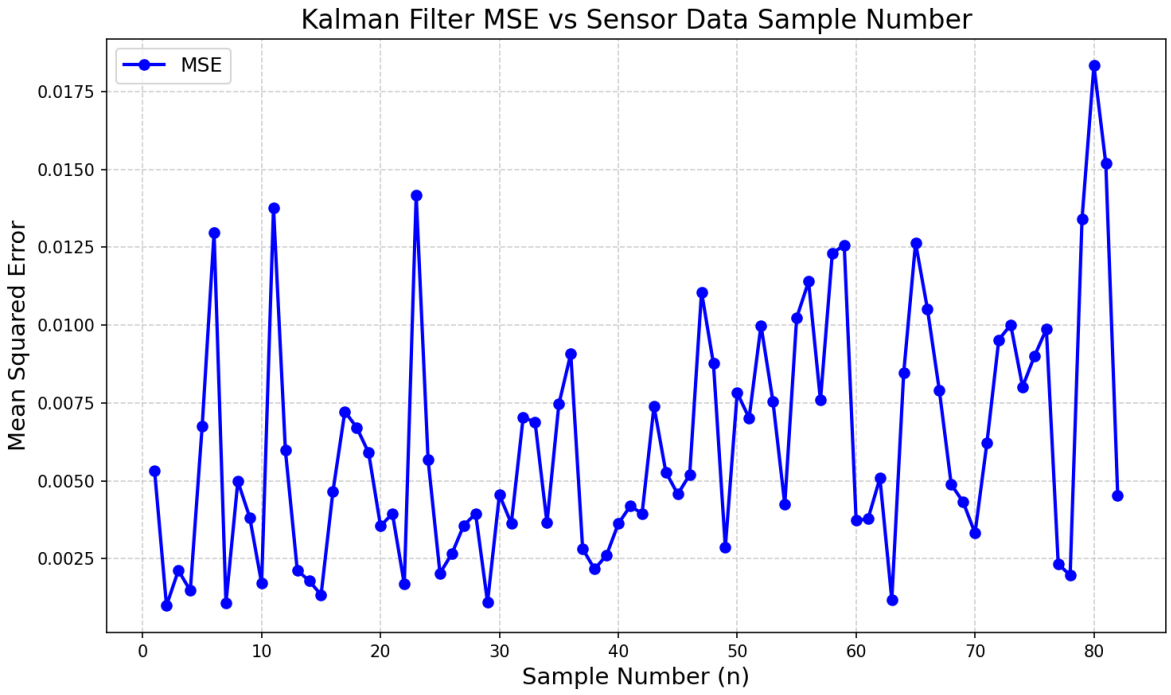
Kalman Filter MSE vs Sensor Data Sample Number
MSE
Mean Squared Error
0.0175
0.0150
0.0125
0.0100
0.0075
0.0050
0.0025
0
10
20
30
40
50
60
70
80
Sample Number (n)

Fig. 4.

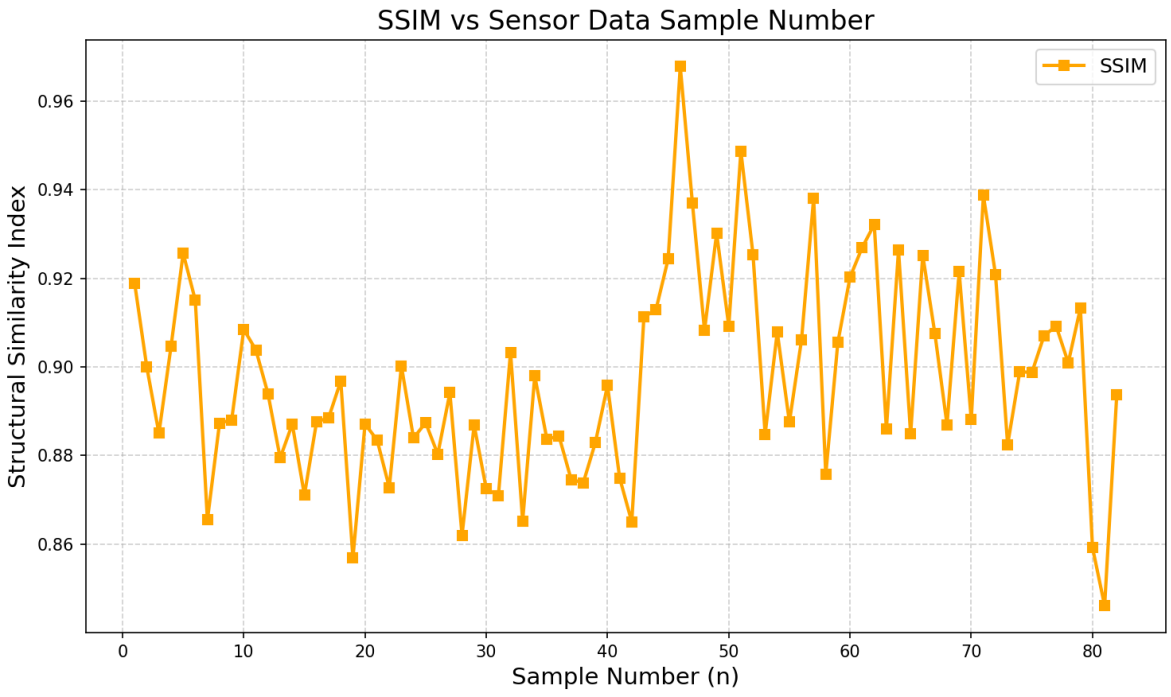
SSIM vs Sensor Data Sample Number
SSIM
Structural Similarity Index
0.96
0.94
0.92
0.90
0.88
0.86
0
10
20
30
40
50
60
70
80
Sample Number (n)

Fig. 5.

Jpn. J. Appl. Phys. **REGULAR PAPER**

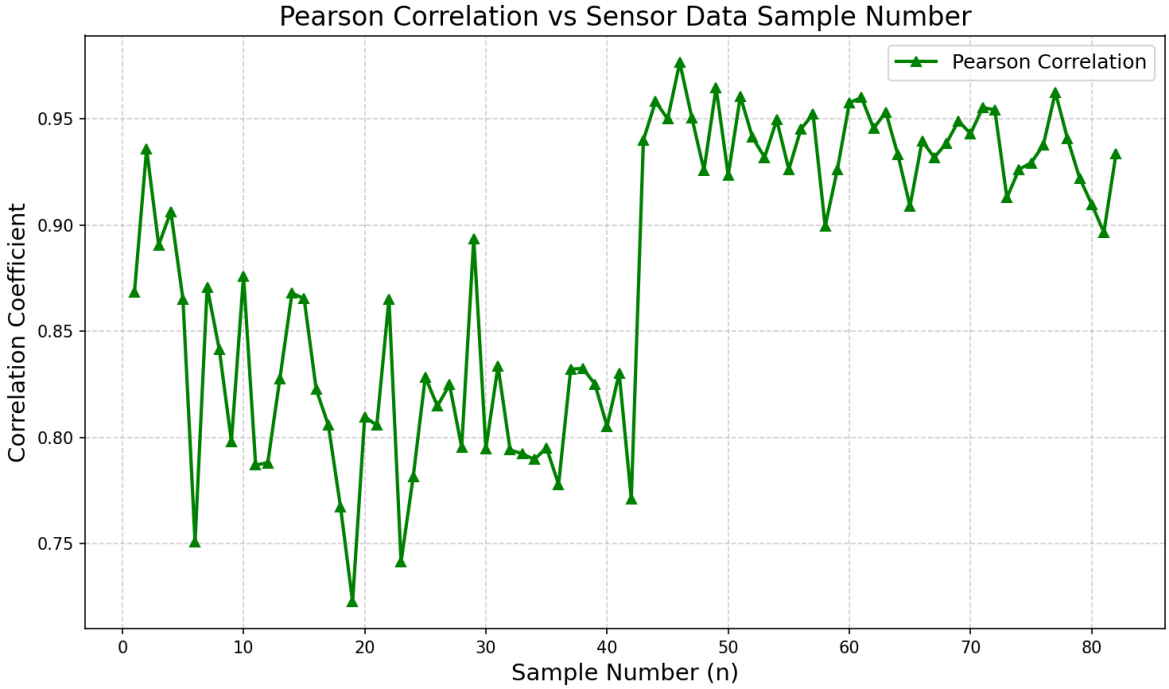

Fig. 6.